Information Sciences Letters
An International Journal

http://dx.doi.org/10.18576/isl/120305

Effects of Porosity, Rotation, Thermomagnetic, and Thickness Variation on Functionally Graded Tapered Annular Disks

R. M. Tantawy[1,*] *and A. M. Zenkour*[2]

[1]Department of Mathematics, Faculty of Science, Damietta University, New Damietta, 34517, Egypt
[2]Department of Mathematics, Faculty of Science, Kafrelsheikh University, Kafrelsheikh 33516, Egypt

Received: 2 Jun. 2022, Revised: 22 Sep. 2022, Accepted: 6 Nov. 2022.
Published online: 1 Mar. 2023.

Abstract: This paper presents a study on porous functionally graded piezoelectric (FGP) annular disks. The paper discussed the magneto-electric-hygrothermal effects on rotating variable thickness porous FG annular disks. Material properties coefficients and magnetic permeability are changed in a power function of radius. The disk is subjected to various loading of a uniform magnetic field, hygrothermal effect, and variation of electric potentials and mechanical pressure on the disk. A semi-analytical technique is used to get the mathematical solution of the rotating annular disk. Numerical outcomes are provided to examine the porosity factor and grading index on the rotating of the disk by different four sets of boundary conditions. The results offered a comparison between the porous and non-porous annular disks with various boundary conditions. Finally, the mathematical solution is beneficial to the planning and manufacture of a rotating porous disk influenced by complex loading and conditions.

Keywords: Porosity; functionally graded; rotating disk; varying thickness; magnetic field; piezoelectric; hygrothermal.

1 Introduction

Functionally graded (FG) porous material has widespread observation around the world due to many applications in mechanical engineering, biomedical, aerospace, modern technology, and different industries. Mechanical actions of various designs of porous FG materials are widely investigated. Gupta and Talha [1] studied the stability of FG plates and the relationship between porosity and initial geometric imperfection. Wang and Zu [2] presented the vibrational properties of longitudinally dynamic sigmoid functionally graded (S-FG) disks including porosities. Wang *et al.* [3] examined the free thermal vibration of porous FG cylindrical shells. Nikrad *et al.* [4] displayed porous FG curved beams with various sets of porosity by using the first-order shear deformation theory with nonlinear Green strains. Jabbari *et al.* [5] established an analytical technique of the FG piezoelectric porous hollow sphere to achieve mechanical displacement and thermal and mechanical stress. Mashat *et al.* [6] presented the hygrothermal effect on the bending of porous FG plates resting on elastic foundations. Different analyses and numerical results of porous functionally graded were studied in references [7-16].

Rotating disks with variable thicknesses are very useful in many applications, like optics, rockets, magnetoelastic sensors, superconducting magnetometers, etc. Because different loading of mechanical pressures, electric potentials, thermal conduction, moisture diffusion, and electric field makes the mathematical more complex, more helpful, and applicable in industry. Allam *et al.* [17] discussed a rotating variable-thickness circular disk with bearing coaxial viscoelastic coating and the impact of steady coaxial current. Dai *et al.* [18] presented rotating porous FG magneto-electro-elastic hollow disks with variable thickness in a hygrothermal medium. The grading index is written by the volume fraction of the piezoelectric component, and the porosity that is determined by the volume fraction of all solid components takes several pores into account. Zenkour [19] studied two cases of rotating sandwich solid disks with exponentially graded (EG) core with free and clamped-edge surface conditions. A semi-analytical method for stress distributions in rotating EG and FG annular disks with thickness variations is presented by Allam *et al.* [20]. Bayat *et al.* [21] discussed the magneto-thermo-mechanical response of the rotating FG magnetoelastic variable-thickness annular disk. Moreover, a lot of researchers explain the FG disk with variable thickness [22-29].

This paper is concerned with the electromagnetic effect, thermal conduction, and moisture diffusion on a rotating functionally graded porous disk response by varying thickness. Several forces act on the disk such as mechanical pressures and variations of electric potentials. Firstly, solving the uncouple differential equation of temperature and moisture and then substituting in constitutive relations with the assistance of the electrostatic equations. Secondly, using a semi-analytical procedure to solve the difficult governing differential equation. Numerical outcomes are discussed according to different cases of boundary conditions for mechanical and electric boundary conditions. A comparison between porous

*Corresponding author e-mail: rania_eltantwy@yahoo.com

and perfect disks is presented for every case.

2 Mathematical Description of a Porous FGP Annular Disk

2.1 Numerical Simulation Procedure

Consider an FG porous symmetric annular disk with variable thickness. Whose inner radius a and outer radius b, and assume that the thickness of the disk is small compared to its diameter. The circular disk geometry is considered according to the cylindrical coordinates (r, θ, z). The geometric disk profile is taken to vary along the radius direction as:

$$h(r) = h_0 \, \mathrm{e}^{-l\left(\frac{r}{b}\right)^k}, \tag{1}$$

where h_0 denotes the thickness at the axis of the disk, l, and k are geometric parameters. Fig. 1 displays the disk profile with different values of l and k.

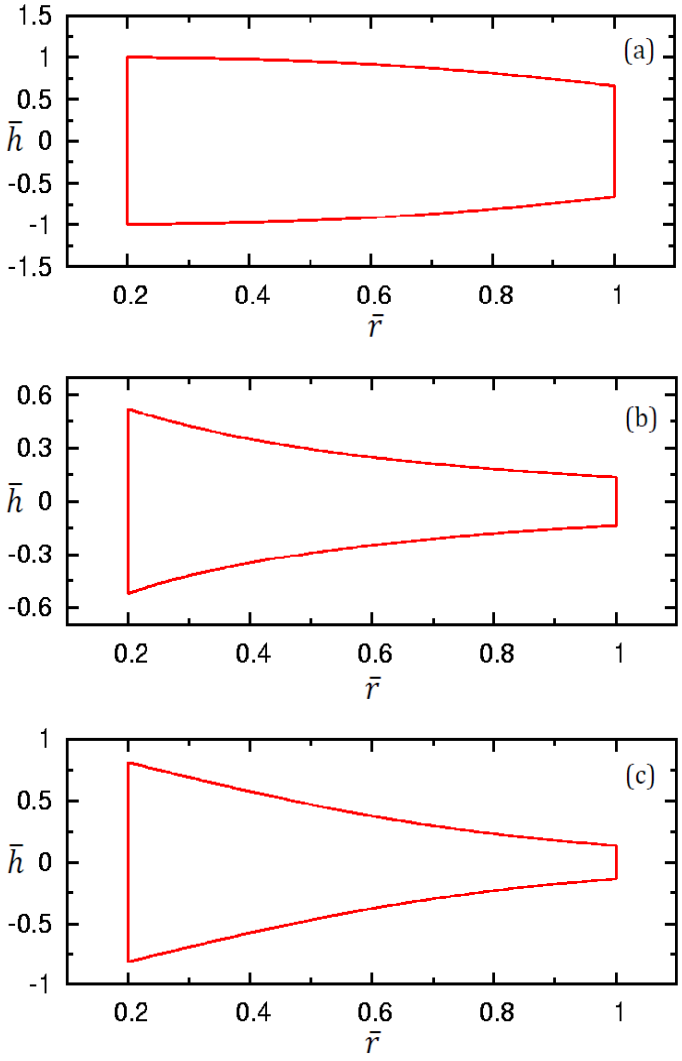

Fig. 1: Exponential disk shape (a) $\boldsymbol{l = 0.4568}$, $\boldsymbol{k = 3}$, (b) $\boldsymbol{l = 2}$, $\boldsymbol{k = 0.7}$ and (c) $\boldsymbol{l = 2}$, $\boldsymbol{k = 1.4}$.

2.2 Mathematical Grading Function

The article studies the mathematical porous FGP annular rotating disk with variable thickness response by mechanical pressure and electric potential in a uniform magnetic field and hygrothermal environment. The porous (FGP) annular disk is made of PZT-4 on its inner surface and made of Cadmium selenide on its outer one. Table 1 reported the material constants of the annular disk.

Assume that the variation of material properties of FGP annular disk with porosity is obeyed by a power law $P(r)$ in the format:

$$P(r) = \left(p^{(b)} - p^{(a)}\right)\left(\frac{r-a}{b-a}\right)^{n} + p^{(a)} - \frac{\beta}{2}\left(p^{(a)} + p^{(b)}\right), \tag{2}$$

where $p^{(a)}$ and $p^{(b)}$ are the properties of internal and external surfaces; a and b are the internal and external radius, respectively; $n \geq 0$ represents the volume fraction exponent (n is the grading index), and $0 \leq \beta \leq 1$ denotes a porosity volume function which vanishes for non-porous structure ($\beta = 0$).

Table 1: Matter constants for PZT-4 and Cadmium selenide.

PZT-4 [31]	Cadmium selenide [32]
$c_{rr}^{(a)} = 115 \times 10^{9}$ (Pa)	$c_{rr}^{(b)} = 83.6 \times 10^{9}$ (Pa)
$c_{r\theta}^{(a)} = 74.3 \times 10^{9}$ (Pa)	$c_{r\theta}^{(b)} = 39.3 \times 10^{9}$ (Pa)
$c_{\theta\varphi}^{(a)} = 77.8 \times 10^{9}$ (Pa)	$c_{\theta\varphi}^{(b)} = 45.2 \times 10^{9}$ (Pa)
$c_{\theta\theta}^{(a)} = 139 \times 10^{9}$ (Pa)	$c_{\theta\theta}^{(b)} = 74.1 \times 10^{9}$ (Pa)
$e_{rr}^{(a)} = 15.1$ (Cm^{-2})	$e_{rr}^{(b)} = 0.347$ (Cm^{-2})
$e_{r\theta}^{(a)} = -5.2$ (Cm^{-2})	$e_{r\theta}^{(b)} = 0.16$ (Cm^{-2})
$\varepsilon_{rr}^{(a)} = 3.87 \times 10^{-9}$ ($\mathrm{C}^{2}\mathrm{K}^{-1}\mathrm{m}^{2}$)	$\varepsilon_{rr}^{(b)} = 9.03 \times 10^{-11}$ ($\mathrm{C}^{2}\mathrm{K}^{-1}\mathrm{m}^{2}$)
$p_{11}^{(a)} = -2.5 \times 10^{-5}$ ($\mathrm{CK}^{-1}\mathrm{m}^{-2}$)	$p_{11}^{(b)} = -2.94 \times 10^{-6}$ ($\mathrm{CK}^{-1}\mathrm{m}^{-2}$)
$\alpha_{r}^{(a)} = 2 \times 10^{-5}$ (K^{-1})	$\alpha_{r}^{(b)} = 2.458 \times 10^{-6}$ (K^{-1})
$\alpha_{\theta}^{(a)} = 2 \times 10^{-6}$ (K^{-1})	$\alpha_{\theta}^{(b)} = 4.396 \times 10^{-6}$ (K^{-1})
$\eta_{r}^{(a)} = 0.03 \times c_{rr}^{(a)}$ ($\mathrm{m}^{3}\mathrm{kg}^{-1}\mathrm{Pa}$)	$\eta_{r}^{(b)} = 0.03 \times c_{rr}^{(b)}$ ($\mathrm{m}^{3}\mathrm{kg}^{-1}\mathrm{Pa}$)
$\eta_{\theta}^{(a)} = 0$ ($\mathrm{m}^{3}\mathrm{kg}^{-1}\mathrm{Pa}$)	$\eta_{\theta}^{(b)} = 0$ ($\mathrm{m}^{3}\mathrm{kg}^{-1}\mathrm{Pa}$)
$\mu^{(a)} = 4\pi \times 10^{-7}(\mathrm{Hm}^{-1})$	$\mu^{(b)} = 6.15 \times 10^{-5}(\mathrm{Hm}^{-1})$
$\rho^{(a)} = 7500(\mathrm{kg\,m}^{-3})$	$\rho^{(b)} = 5684(\mathrm{kg\,m}^{-3})$

2.3 Hygrothermal Equations and Conditions

The equations of temperature and moisture are assumed to be graded in the radial direction of the annular disk. Fourier heat equation and Fickian moisture diffusion along the radial direction can be written as (Paria [30], Bayat *et al.* [21])

$$\left.\begin{aligned} \frac{1}{rh(r)}\frac{\mathrm{d}}{\mathrm{d}r}\left(r\,k_T\,h(r)\frac{\mathrm{d}T(r)}{\mathrm{d}r}\right) = 0, \\ \frac{1}{rh(r)}\frac{\mathrm{d}}{\mathrm{d}r}\left(r\,k_C\,h(r)\frac{\mathrm{d}C(r)}{\mathrm{d}r}\right) = 0, \end{aligned}\right\} \tag{3}$$

where k_T, k_C are the mean of the heat conductivity constant and the mean of the moisture diffusion constant, respectively.

The boundary conditions for temperature and moisture are written in the form

$$\left.\begin{aligned} T(r)|_{r=a} = T_0, \quad T(r)|_{r=b} = T_1, \\ C(r)|_{r=a} = 0, \quad C(r)|_{r=b} = C_0, \end{aligned}\right\} \tag{4}$$

where T_0 is reference temperature, C_0 is the initial moisture concentration and T_1 is the temperature at r=b.

By solving the differential Eqs. (3) one gets

$$\begin{aligned} T(r) &= c_1 - c_2 Ei(1, -l\,r^{k}), \\ C(r) &= c_3 - c_4 Ei(1, -l\,r^{k}), \end{aligned} \tag{5}$$

where $Ei(a, z)$ are the exponential integral defined in the form

$$Ei(a, z) = z^{a-1}\Gamma(1 - a, z), \tag{6}$$

and c_1, c_2, c_3, c_4 are unknown constants for temperature and moisture equations, applying the boundary conditions (4)

$$\left.\begin{aligned} c_1 &= \frac{T_1 Ei(1,-l\,a^k)-T_0 Ei(1,-l\,b^k)}{Ei(1,-l\,a^k)-Ei(1,-l\,b^k)},\\ c_2 &= \frac{T_1-T_0}{Ei(1,-l\,a^k)-Ei(1,-l\,b^k)},\\ c_3 &= \frac{C_0 Ei(1,-l\,a^k)}{Ei(1,-l\,a^k)-Ei(1,-l\,b^k)},\\ c_4 &= \frac{C_0}{Ei(1,-l\,a^k)-Ei(1,-l\,b^k)}. \end{aligned}\right\} \tag{7}$$

2.4 Constitutive and Equilibrium Differential Equations

The porous functionally graded annular disk with variable thickness is responded by a computation of actions consisting of moisture diffusion $C(r)$, temperature distribution $T(r)$ and electric potential $\psi(r)$ is located in a uniform magnetic field. The constitutive equations for the mathematical porous FGP model are written in the form (Dai and Dai [26], Dai and Jiang [33], Dai *et al.* [34])

$$\begin{Bmatrix}\sigma_r\\ \sigma_\theta\end{Bmatrix} = \begin{bmatrix} c_{rr} & c_{r\theta} & e_{rr}\\ c_{r\theta} & c_{\theta\theta} & e_{r\theta}\end{bmatrix}\begin{Bmatrix}\frac{\mathrm{d}u}{\mathrm{d}r}\\ \frac{u}{r}\\ \frac{\mathrm{d}\psi}{\mathrm{d}r}\end{Bmatrix} - \begin{Bmatrix}\lambda_r\\ \lambda_\theta\end{Bmatrix}T(r) - \begin{Bmatrix}\eta_r\\ \eta_\theta\end{Bmatrix}C(r), \tag{8}$$

and electric displacement is

$$D_r = e_{rr}\frac{\mathrm{d}u}{\mathrm{d}r} + e_{r\theta}\frac{u}{r} - \varepsilon_{rr}\frac{\mathrm{d}\psi}{\mathrm{d}r} + p_{11}T(r) + p_{22}C(r), \tag{9}$$

where $e_{rj}\ (j=r,\theta)$, $c_{ij}\ (i,j=r,\theta,z)$, $\eta_i\ (i=r,\theta)$, ε_{rr}, p_{11} and p_{22} and denote piezoelectric, elastic, moisture expansion, dielectric, pyroelectric and hygroelectric coefficients, while λ_i related to the material coefficients in the forms

$$\begin{Bmatrix}\lambda_r\\ \lambda_\theta\end{Bmatrix} = \begin{bmatrix} c_{rr} & c_{r\theta}\\ c_{r\theta} & c_{\theta\theta}\end{bmatrix}\begin{Bmatrix}\alpha_r\\ \alpha_\theta\end{Bmatrix}T(r) - \begin{Bmatrix}\eta_r\\ \eta_\theta\end{Bmatrix}C(r), \tag{10}$$

where α_i are the thermal expansion coefficients and η_i are the moisture expansion constants described by

$$\begin{Bmatrix}\eta_r\\ \eta_\theta\end{Bmatrix} = \begin{bmatrix} c_{rr} & c_{r\theta}\\ c_{r\theta} & c_{\theta\theta}\end{bmatrix}\begin{Bmatrix}\delta_r\\ \delta_\theta\end{Bmatrix}. \tag{11}$$

Consider the magnetic permeability $\mu(r)$ of porous FGP annular disk are the same as the magnetic permeability of its environment (Ezzat [35]). The specifications properties of the medium are non-ferromagnetic and non-ferroelectric with neglect of Thompson influence. Maxwell's equations of electrodynamics are written as (Kraus [36], Dai and Wang [37])

$$\begin{aligned} &\underline{J} = \nabla\times\underline{v}, \quad \nabla\times\underline{e} = -\mu\frac{\partial\underline{v}}{\partial t},\\ &\nabla\cdot\underline{v} = 0, \quad \underline{e} = -\mu\left(\frac{\partial\underline{u}}{\partial t}\times\underline{H}\right),\\ &\underline{v} = \nabla\times\left(\underline{u}\times\underline{H}\right). \end{aligned} \tag{12}$$

The vector of primary magnetic $\underline{H}\equiv(0,0,H)$ and displacement field $\underline{u}\equiv(u,0,0)$ while $\underline{v}\equiv(0,0,v)$, offset in Eq. (12)

$$\begin{aligned} \underline{e} &= -\mu(r)\left(0, H\frac{\partial u}{\partial t}, 0\right),\\ \underline{J} &= \left(0, -\frac{\partial v}{\partial r}, 0\right),\\ v &= -H\left(\frac{\partial u}{\partial r}+\frac{2u}{r}\right), \end{aligned} \tag{13}$$

where H is a uniform magnetic field. As a rule, postulate that c_{ij}, e_{rj}, α_i, η_i, μ, p_{11} and p_{22} of the porous rotating annular disk obey the power gradation law in Eq. (1).

The equilibrium differential equations by considering symmetry and the inertia and Lorentz force of an FGP porous annular disk are expressed as:

$$\begin{aligned} &\frac{\mathrm{d}}{\mathrm{d}r}(h(r)\sigma_r) + \frac{h(r)}{r}(\sigma_r-\sigma_\theta) + h(r)(F_r+F_H) = 0,\\ &F_r = \rho\omega^2 r,\\ &F_H = \mu(r)\left(\underline{J}\times\underline{H}\right) = H^2\frac{\partial}{\partial r}\left(\mu\frac{du}{dr}+\mu\frac{nu}{r}\right), \end{aligned} \tag{14}$$

where F_r, F_H are the inertia and Lorentz forces, respectively, and Maxwell's equation for an annular rotating disk with variable thickness is

$$\frac{\mathrm{d}}{\mathrm{d}r}(h(r)D_r)+\frac{h(r)}{r}D_r=0, \tag{15}$$

where D_r represents electric displacement.

3 Semi-analytical Technique for FGP Porous Annular Disk

The semi-analytical solution for a rotating FGP porous annular disk with variable thickness is gained by solving the uncoupled hygrothermal equations, Eq. (3) at first, and the next step solves the equilibrium and Maxwell's equations subjected to mechanical and electric boundary conditions.

The temperature distribution and moisture diffusion equations shown in Eqs. (5), and the electric displacement solution of Eq. (15) is expressed in the form

$$D_r=\frac{A_1}{r\,h(r)}, \tag{16}$$

where A_1 is an integration constant. Then, the electric potential function with the aid of Eqs. (9), (16), and the graded relation (2), yields

$$\frac{\mathrm{d}\psi}{\mathrm{d}r}=\frac{1}{\varepsilon_{rr}}\left(e_{rr}\frac{\mathrm{d}u}{\mathrm{d}r}+e_{r\theta}\frac{u}{r}+p_{11}T(r)+p_{22}C(r)-\frac{A_1}{r\,h(r)}\right). \tag{17}$$

By substituting in equilibrium differential equation (13) and gathering the terms of a different order of radial displacement derivatives as

$$\begin{aligned}&\frac{\mathrm{d}^2u}{\mathrm{d}r^2}+\left(\frac{h(r)\frac{\mathrm{d}m_{11}}{\mathrm{d}r}+m_{11}\frac{dh(r)}{dr}+h(r)H^2\frac{d\mu}{dr}}{h(r)(m_{11}+\mu H^2)}+\frac{1}{r}\right)\frac{\mathrm{d}u}{\mathrm{d}r}+\left(\frac{h(r)\frac{\mathrm{d}m_{12}}{\mathrm{d}r}+m_{12}\frac{dh(r)}{dr}+h(r)H^2\frac{d\mu}{dr}}{rh(r)(m_{11}+\mu H^2)}-\frac{m_{22}+\mu H^2}{r^2(m_{11}+\mu H^2)}\right)u\\&+\left(\frac{h(r)\frac{\mathrm{d}m_{41}}{\mathrm{d}r}+m_{41}\frac{dh(r)}{dr}}{h(r)(m_{11}+\mu H^2)}+\frac{(m_{41}-m_{42})}{r(m_{11}+\mu H^2)}\right)C(r)+\left(\frac{h(r)\frac{\mathrm{d}m_{31}}{\mathrm{d}r}+m_{31}\frac{dh(r)}{dr}}{h(r)(m_{11}+\mu H^2)}+\frac{(m_{31}-m_{32})}{r(m_{11}+\mu H^2)}\right)T(r)\\&+\frac{m_{31}}{m_{11}+\mu H^2}\frac{\mathrm{d}T}{\mathrm{d}r}+\frac{m_{41}}{m_{11}+\mu H^2}\frac{\mathrm{d}C}{\mathrm{d}r}-\left(\frac{\frac{\mathrm{d}m_{51}}{\mathrm{d}r}}{rh(r)(m_{11}+\mu H^2)}-\frac{m_{52}}{r^2h(r)(m_{11}+\mu H^2)}\right)A_1+\frac{\rho\omega^2 r}{h(r)(m_{11}+\mu H^2)}=0,\end{aligned} \tag{18}$$

where m_{ij} are functions of r

$$\left.\begin{aligned}&m_{11}=c_{rr}+\frac{e_{rr}e_{rr}}{\varepsilon_{rr}},\quad m_{12}=c_{r\theta}+\frac{e_{rr}e_{r\theta}}{\varepsilon_{rr}},\quad m_{22}=c_{\theta\theta}+\frac{e_{r\theta}e_{r\theta}}{\varepsilon_{rr}},\\&m_{31}=\frac{e_{rr}p_{11}}{\varepsilon_{rr}}-\lambda_r,\quad m_{32}=\frac{e_{r\theta}p_{11}}{\varepsilon_{rr}}-\lambda_\theta,\quad m_{41}=\frac{e_{rr}p_{22}}{\varepsilon_{rr}}-\eta_r,\\&m_{42}=\frac{e_{r\theta}p_{22}}{\varepsilon_{rr}}-\eta_\theta,\quad m_{51}=\frac{e_{rr}}{\varepsilon_{rr}},\quad m_{52}=\frac{e_{r\theta}}{\varepsilon_{rr}}.\end{aligned}\right\} \tag{19}$$

To finish the mathematical solution after obtaining the general solution of radial displacement in Eq. (18), substitute in Eq. (17), and integrate with more integration constant A_2 to gain the electric potential function $\psi(r)$.

The boundary mechanical and electric conditions on FGP porous annular disk with variable thickness are:

$$\begin{aligned}&\sigma_r|_{r=a}=-P_1,\quad \sigma_r|_{r=b}=-P_2,\\&\psi(r)|_{r=a}=\psi_1,\quad \psi(r)|_{r=b}=\psi_2,\end{aligned} \tag{20}$$

where P_1, P_2 are the pressures on the inner and outer surface of the disk and ψ_1, ψ_2 are the values of electric potentials on internal and external radii.

The completion of the radial displacement distribution of Eq. (18) as a function of variable r is difficult. So, it is suitable to utilize a semi-analytical method to obtain the solution of the differential equation (18). In this technique, the radial range is split into some virtual divisions with a thickness $s^{(k)}$, as presented in Fig. 2. The evaluation of the factors of Eq. (18) at $r=r^{(k)}$, the mean radius of the kth portion, and utilizing them as suitable variable coefficients in Eq. (18), that is

$$\frac{\mathrm{d}^2u^{(k)}}{\mathrm{d}r^2}+N_1^{(k)}\frac{\mathrm{d}u^{(k)}}{\mathrm{d}r}+N_2^{(k)}u^{(k)}+N_3^{(k)}=0, \tag{21}$$

where

$$N_1^{(k)} = \left.\frac{h(r)\frac{\mathrm{d}m_{11}}{\mathrm{d}r}+m_{11}\frac{dh(r)}{dr}+h(r)H^2\frac{d\mu}{dr}}{h(r)(m_{11}+\mu H^2)}\right|_{r=r^{(k)}} + \frac{1}{r^{(k)}},$$

$$N_2^{(k)} = \left.\frac{h(r)\frac{\mathrm{d}m_{12}}{\mathrm{d}r}+m_{12}\frac{dh(r)}{dr}+h(r)H^2\frac{d\mu}{dr}}{rh(r)(m_{11}+\mu H^2)}\right|_{r=r^{(k)}} - \left.\frac{m_{22}+\mu H^2}{r^2(m_{11}+\mu H^2)}\right|_{r=r^{(k)}},$$

$$N_3^{(k)} = \left.\frac{m_{41}}{m_{11}+\mu H^2}\right|_{r=r^{(k)}} \left.\frac{\mathrm{d}C}{\mathrm{d}r}\right|_{r=r^{(k)}} + \left(\left.\frac{h(r)\frac{\mathrm{d}m_{41}}{\mathrm{d}r}+m_{41}\frac{dh(r)}{dr}}{h(r)(m_{11}+\mu H^2)}\right|_{r=r^{(k)}} + \left.\frac{(m_{41}-m_{42})}{r(m_{11}+\mu H^2)}\right|_{r=r^{(k)}}\right) C\left(r^{(k)}\right)$$

$$+ \left.\frac{m_{31}}{m_{11}+\mu H^2}\right|_{r=r^{(k)}} \left.\frac{\mathrm{d}T}{\mathrm{d}r}\right|_{r=r^{(k)}} + \left(\left.\frac{h(r)\frac{\mathrm{d}m_{31}}{\mathrm{d}r}+m_{31}\frac{dh(r)}{dr}}{h(r)(m_{11}+\mu H^2)}\right|_{r=r^{(k)}} + \left.\frac{(m_{31}-m_{32})}{r(m_{11}+\mu H^2)}\right|_{r=r^{(k)}}\right) T\left(r^{(k)}\right)$$

$$- \left(\left.\frac{\frac{\mathrm{d}m_{51}}{\mathrm{d}r}}{rh(r)(m_{11}+\mu H^2)}\right|_{r=r^{(k)}} - \left.\frac{m_{52}}{r^2h(r)(m_{11}+\mu H^2)}\right|_{r=r^{(k)}}\right) A_1^{(k)} + \left.\frac{\rho\omega^2 r}{h(r)(m_{11}+\mu H^2)}\right|_{r=r^{(k)}}, \tag{22}$$

while m_{ij} are functions of $r^{(k)}$. By using the semi-analytical approach, Eq. (18) with variable factors is wide-ranging into a system of m differential equations with constant factors and m is the number of virtual divisions. The radial displacement as a function of r can be written in the format

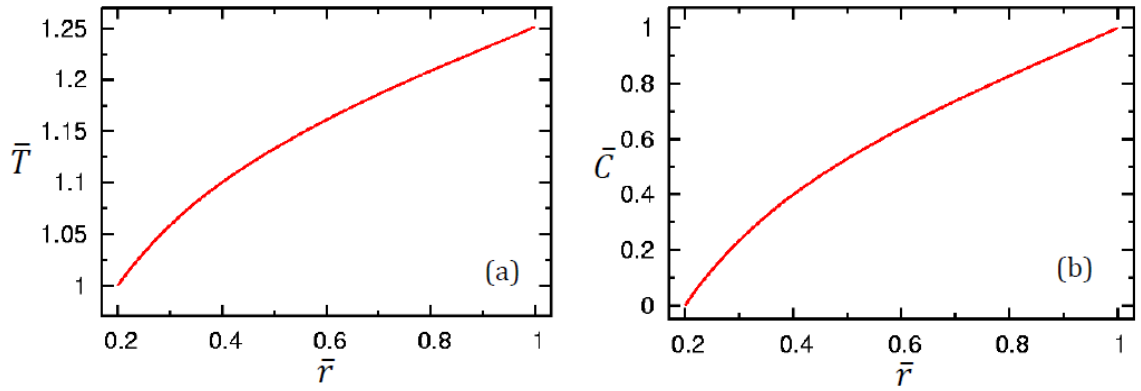

Fig. 2: Temperature distribution and moisture diffusion in porous FGP annular disk.

$$u^{(k)} = B_1^{(k)}\mathrm{e}^{\delta_1 r} + B_2^{(k)}\mathrm{e}^{\delta_2 r} - \frac{N_3^{(k)}}{N_2^{(k)}}, \tag{23}$$

where δ_1, δ_2 denote the roots of the algebraic equation $\delta^2 + N_1^{(k)}\delta + N_2^{(k)} = 0$, and $B_1^{(k)}$ and $B_2^{(k)}$ are constants of the differential equation (18) for the kth sub-domain. Also, the radial displacement solution Eq. (23) is standing for

$$r^{(k)} - \frac{s^{(k)}}{2} \le r \le r^{(k)} + \frac{s^{(k)}}{2}, \tag{24}$$

where $r^{(k)}$ and $s^{(k)}$ are the mean radius and the portion thickness of the kth division, respectively. The constants $B_1^{(k)}$ and $B_2^{(k)}$ specified from the continuity conditions between every two-neighboring division. So, the continuity conditions are imposed at the interfaces of neighboring sub-domains in the form:

$$\begin{aligned}
&u^{(k)}\big|_{r=r^{(k)}+\frac{s^{(k)}}{2}} = u^{(k+1)}\big|_{r=r^{(k+1)}-\frac{s^{(k+1)}}{2}},\\
&\sigma_r^{(k)}\big|_{r=r^{(k)}+\frac{s^{(k)}}{2}} = \sigma_r^{(k+1)}\big|_{r=r^{(k+1)}-\frac{s^{(k+1)}}{2}},\\
&\sigma_\theta^{(k)}\big|_{r=r^{(k)}+\frac{s^{(k)}}{2}} = \sigma_\theta^{(k+1)}\big|_{r=r^{(k+1)}-\frac{s^{(k+1)}}{2}},\\
&\psi^{(k)}\big|_{r=r^{(k)}+\frac{s^{(k)}}{2}} = \psi^{(k+1)}\big|_{r=r^{(k+1)}-\frac{s^{(k+1)}}{2}}.
\end{aligned} \tag{25}$$

Using the continuity equations (25), mechanical and electric boundary conditions to get a system of linear equations in constants $A_1^{(k)}, A_2^{(k)}, B_1^{(k)}, B_2^{(k)}$, $(k = 1,2,\ldots,m)$. By getting the constants, we can set the radial displacement in each subdomain. The increase in the number of sub-domains improves better rigor of the outcomes.

4 Numerical Investigation

To verify the theoretical study, a numerical investigation is presented in Figs. 3-11 and Tables 2-9 to illustrate the influence of porosity factor, hygrothermal distribution, mechanical pressures, and an electric potential on a porous FGP porous annular rotating disk with variable thickness. The numerical outcomes are carried out for porous and perfect annular disks, and different mechanical and electric forces. Suppose the internal and external radius of a porous annular disk is $a = 0.2$ (m), $b = 1$ (m), $l = 0.4568$, and $k = 3$.

The dimensionless rules are:

$$\bar{r} = \frac{r}{b}, \quad \bar{u} = \frac{u}{b} \times 10^2, \quad \bar{T} = \frac{T(\bar{r})}{T_0}, \quad \bar{C} = \frac{C(\bar{r})}{C_0}, \tag{26}$$

while the dimensionless for radial and hoop stresses and electric potential will be written for every example.

Consider PZT-4 and Cadmium selenide are the material of internal and external surfaces, respectively. The materials constants are shown in Table 1 (Ootao and Tanigawa [31], Ghorbanpour *et al.* [32]).

The mechanical and electric potentials boundary conditions are studied, sequentially:

Example 1: $P_1 = 0$ (Pa), $P_2 = 0$ (Pa), $\psi_1 = 0$ (W/A), $\psi_2 = 0$ (W/A). (27)

Example 2: $P_1 = 0$ (Pa), $P_2 = 10^{10}$ (Pa), $\psi_1 = 0$ (W/A), $\psi_2 = 0$ (W/A). (28)

Example 3: $P_1 = 0$ (Pa), $P_2 = 0$ (Pa), $\psi_1 = 10^8$ (W/A), $\psi_2 = 0$ (W/A). (29)

Example 4: $P_1 = 10^{10}$ (Pa), $P_2 = 0$ (Pa), $\psi_1 = 0$ (W/A), $\psi_2 = 10^8$ (W/A). (30)

Figure 1 displays the exponential disk profile for various values of geometric parameters l, k for $l = 0.4568$, $k = 3$, $l = 2$, $k = 0.7$, and $l = 2$, $k = 1.4$. Figure 2 presents temperature and moisture distribution along the radial direction of the rotating annular disk. Fig. 2(a) illustrates the temperature attitude in FGP porous annular disk. The temperature satisfies the boundary conditions for temperature on inner and outer surfaces. Temperature curve increases adjacent to the radial direction and has the maximum value at the external surface of the porous annular disk. Fig. 2(b) presents the moisture diffusion of the porous disk. The humidity increases from zero on the inner surface to one on the outer ones obeying the moisture boundary conditions. Figure 3 presents a diagram for the semi-analytical technique and how to allocate the radial range into some virtual divisions.

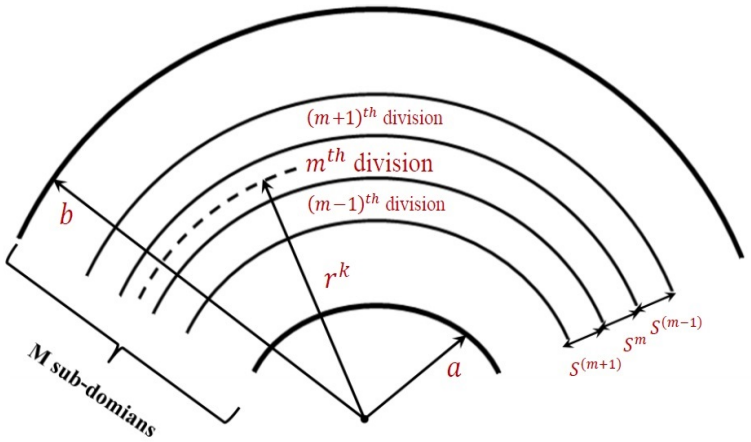

Fig. 3: Splitting radial range into some virtual sub-divisions.

4.1 Example 1: Free-Free Conditions

Assume that the mechanical and electrical loading on surfaces of the FGP porous annular disk equals zero. Suppose that the dimensionless stresses and electric potential in this example are in the form:

$$\{\bar{\sigma}_r, \bar{\sigma}_\theta, \bar{\psi}\} = \{\sigma_r, \sigma_\theta, \psi\}. \tag{31}$$

Table 2 compares the perfect FGP annular disk for $(\beta = 0)$ and porous FGP disk for $(\beta = 0.2)$ for different values of grading index $n = 5$, 10, 20. The comparison of various positions on the annular disk for dimensionless displacement $\bar{u}$, radial stress $\bar{\sigma}_r$, hoop stress $\bar{\sigma}_\theta$ and electric potential $\bar{\psi}$. Notice that from the table all values of displacement, stresses, and electric potentials in a perfect FGP annular rotating disk are greater than values in FGP porous annular disk.

Table 2: Effects of porosity parameter and grading index on FGP porous annular disk without electrical load on the internal surface and mechanical on the external surface.

Variable	$\bar{r}$	Perfect FGPM ($\beta = 0$)			Porous FGPM ($\beta = 0.2$)		
		$n = 5$	$n = 10$	$n = 20$	$n = 5$	$n = 10$	$n = 20$
$\bar{u}$	0.3	1.2722	0.8023	0.4766	0.7543	0.4132	-148.04
	0.5	1.3372	1.0376	0.8302	0.9830	0.7634	-101.06
	0.7	1.5520	1.3417	1.1998	1.2873	1.1287	-77.130
$\bar{\sigma}_r$	0.3	0.1809	0.1320	0.0982	0.1024	0.0717	-14.238
	0.5	0.2340	0.1901	0.1592	0.1467	0.1187	-14.413
	0.7	0.1985	0.1767	0.1577	0.1320	0.1176	-10.963
$\bar{\sigma}_\theta$	0.3	0.4965	0.4033	0.3389	0.3158	0.2569	-28.579
	0.5	0.3804	0.3640	0.3526	0.2889	0.2778	-8.5000
	0.7	0.3398	0.3489	0.3539	0.2785	0.2834	-2.4757
$\bar{\psi}$	0.3	0.0748	0.0241	-0.0111	0.0360	0.0042	-11.556
	0.5	0.2826	0.1322	0.0274	0.1561	0.0586	-37.475
	0.7	0.4771	0.2544	0.0955	0.2775	0.1357	-58.844

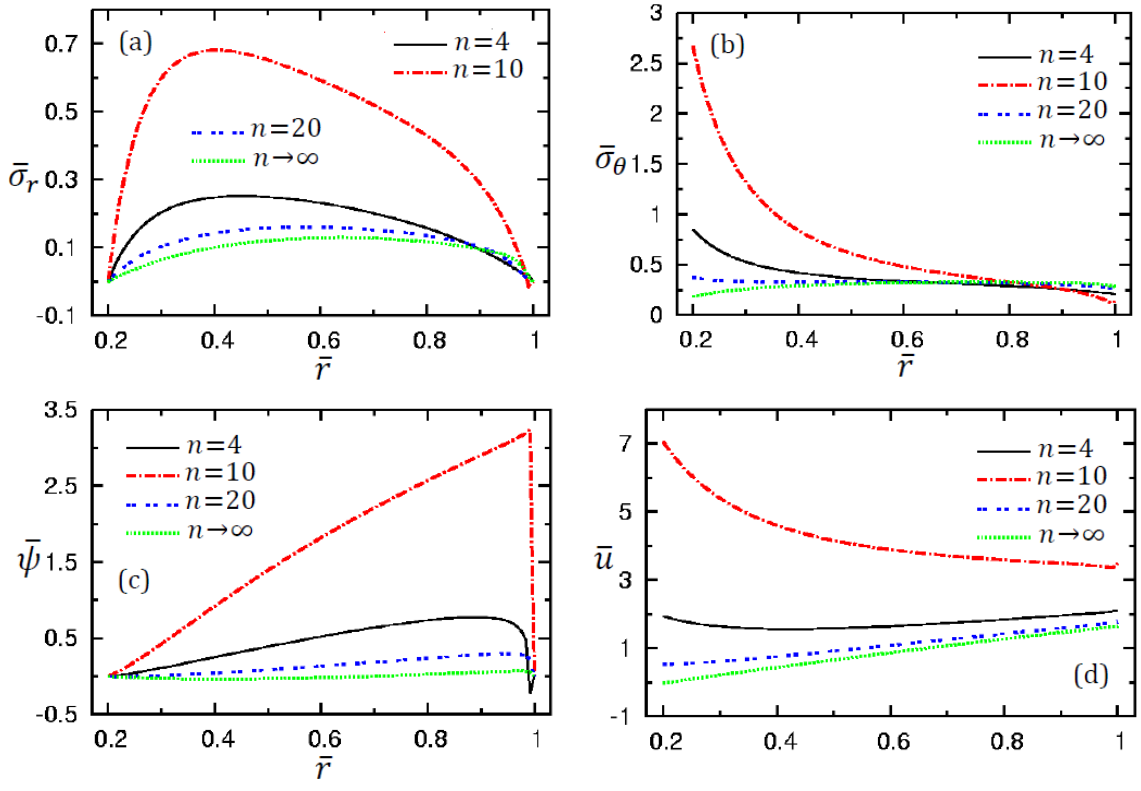

Fig. 4: Grading index effect on stresses, electric potential, and displacement on FGP porous annular disk with free mechanical and free electrical loading.

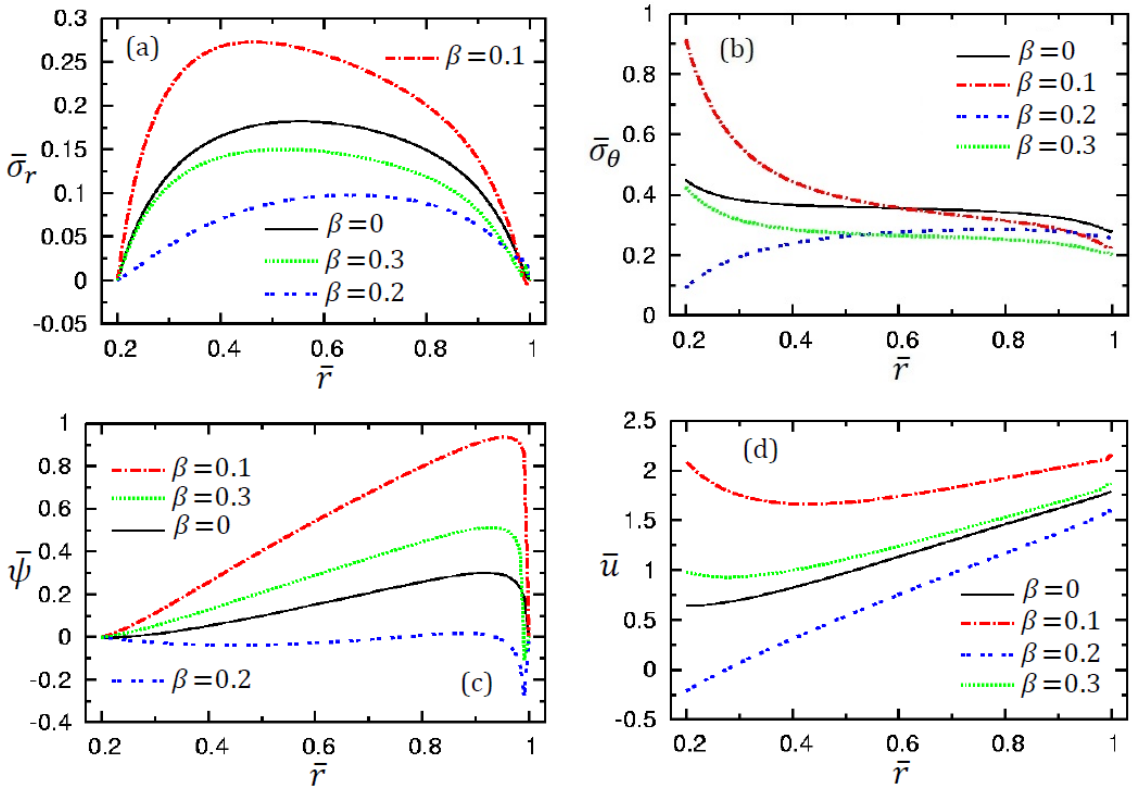

Fig. 5: Porosity parameter effect on stresses, electric potential, and displacement on FGP porous annular disk with free mechanical and free electrical loading.

Figure 4 demonstrates the impact of various grading index values $n = 4, 10, 20$, and $n \to \infty$ on stresses, electric potential, and radial displacement with porosity factor $\beta = 0.1$. Fig. 4(a) presents the radial stress along the radial direction. The radial stress satisfies the mechanical boundary condition. The radial stress increases from $\bar{r} = 0.2$ to $\bar{r} = 0.35$ and then decreases to the external radius. The hoop stress is described in Fig. 4(b). The hoop stress is decreasing from the internal to the external surface of the porous annular disk. The maximum value of the hoop stress appears at $n = 10$ on the inner surface and the minimum value on the outer surface exists at $n = 10$. Fig. 4(c) shows the electric potential of the FGP porous annular disk with various values of grading index. The electric potential increasing and then decreasing along the radial of the disk to satisfy the electric boundary conditions. Fig. 4(d) displays the radial displacement on the FGP porous annular rotating disk with variable thickness. The greatest value happens at the internal surface and the radial displacement decreasing to the external surface in the case of $n = 4$, 10 but in $n = 20$ and $n \to \infty$ the radial displacement increases from the internal to external surfaces.

Figure 5 displays the influence of the porosity factor on stresses, electric potential, and radial displacement with the exact value of grading index $n = 12$ and various values of porosity factor $\beta = 0,0.1,0.2,0.3$. Fig. 5(a) presents the radial stress in the FGP annular disk with various values of porosity factor. The greatest value of radial stress occurs at $\beta = 0.1$ and the minimum value exists at $\beta = 0.2$. The radial stress curves increase from zero value on the internal surface and decrease to zero value on the external surface to satisfy the mechanical boundary conditions. Fig. 5(b) demonstrates the hoop stress on FGP porous annular disk. The hoop stress decreasing from the inner to the outer surface except for $\beta = 0.2$ the hoop stress increase from the internal to the external radius. The electric potential is displayed in Fig. 5(c). The electric potential increasing from the inner surface from zero and decreasing near the external surface to equal zero and satisfy the electric boundary conditions. Fig. 5(d) presents the radial displacement for different values of the porosity factor. The radial displacement increases from the inner to the outer surface. The radial displacement maximum value happens when $\beta = 0.1$ and the lower value when $\beta = 0.2$.

4.2 Example 2: Mechanical-Free Conditions

Assume that there is an external mechanical pressure P_2 and no existence of electric potential on the external surface while the inner surface is free of mechanical and electric potential. In this case, the FGP porous annular rotating disk of

variable thickness is treated as a sensor. The dimensionless in this example takes the form:

$$\{\bar{\sigma}_r, \bar{\sigma}_\theta, \bar{\psi}\} = \left\{\frac{\sigma_r}{P_2}, \frac{\sigma_\theta}{P_2}, \psi\right\}. \quad (32)$$

Table 3: Effects of porosity parameter and grading index on FGP porous annular disk without electrical load on the internal surface and with mechanical pressure on the external.

Variable	$\bar{r}$		Perfect FGPM ($\beta = 0$)			Porous FGPM ($\beta = 0.2$)		
			$n = 5$	$n = 10$	$n = 20$	$n = 5$	$n = 10$	$n = 20$
$\bar{u}$	0.3		0.00344	-0.30887	-0.57586	-0.23644	-0.51951	-118.28
	0.5		-0.02658	-0.21680	-0.38452	-0.17857	-0.35323	-81.119
	0.7		-0.07362	-0.17816	-0.28923	-0.17196	-0.26738	-62.343
$\bar{\sigma}_r$	0.3		-0.04944	-0.08049	-0.10783	-0.06469	-0.08919	-11.437
	0.5		-0.11157	-0.13645	-0.16086	-0.11499	-0.13498	-11.662
	0.7		-0.20957	-0.20318	-0.21592	-0.38981	-0.28300	-8.9711
$\bar{\sigma}_\theta$	0.3		-0.08619	-0.14328	-0.19478	-0.11831	-0.16392	-23.038
	0.5		-0.05818	-0.06278	-0.07049	-0.05988	-0.06279	-7.0245
	0.7		-0.07124	-0.05045	-0.04399	-0.08613	-0.05991	-2.2266
$\bar{\psi}$	0.3		0.15130	0.11447	0.08473	0.12805	0.09945	-9.076
	0.5		0.35653	0.24938	0.16158	0.28737	0.20118	-29.573
	0.7		0.48931	0.33268	0.19987	0.38414	0.25913	-46.528

Table 3 depicts the values of radial displacement, stresses, and electric potential for perfect and porous FGP annular rotating disk with variable thickness for various values of grading index n. From this table, all values clarify that the radial displacement, stresses, and electric potential in the porous annular disk are smaller than the corresponding values in the perfect annular disk.

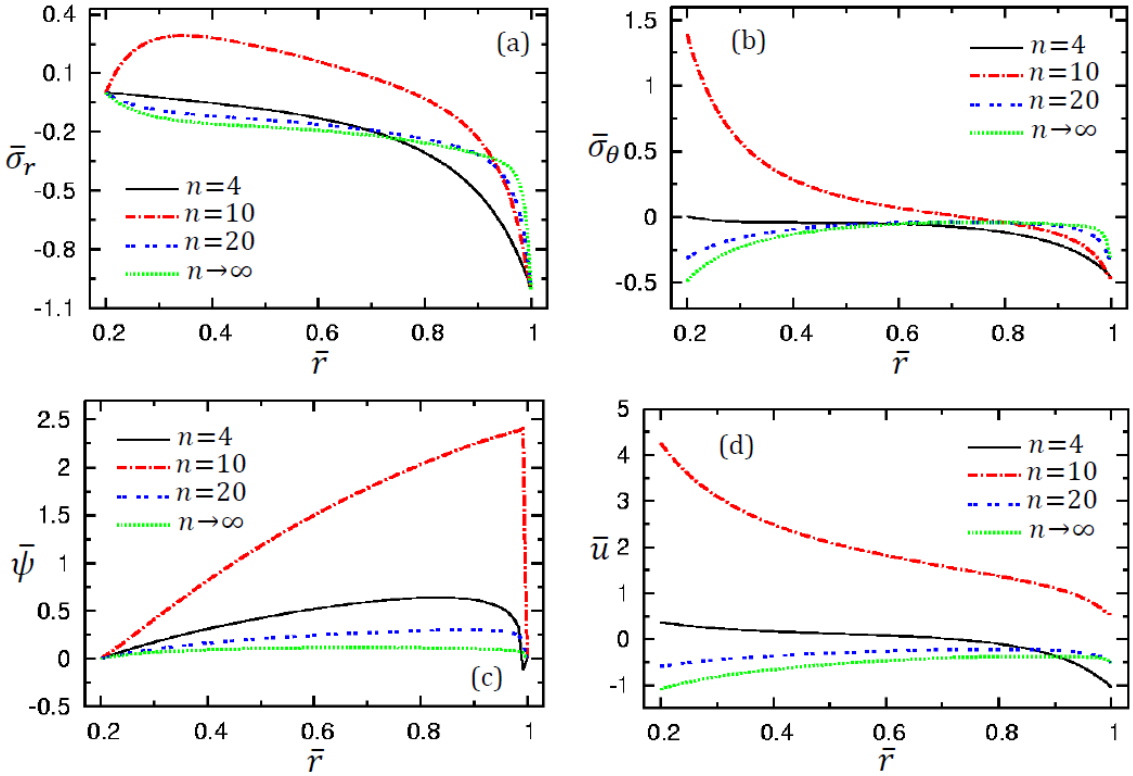

Fig. 6: Grading index effect on stresses, electric potential, and displacement on FGP porous annular disk without electrical load on the inner surface and with mechanical pressure on the outer radius.

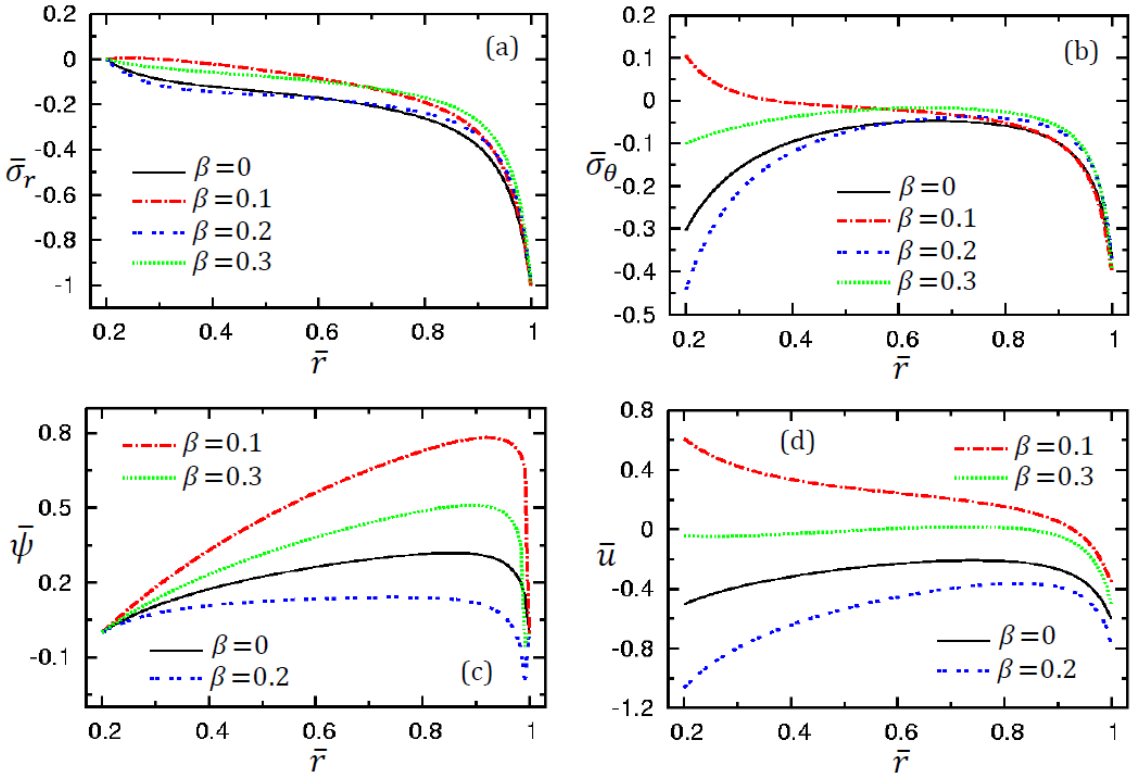

Fig. 7: Porosity parameter effect on stresses, electric potential, and displacement on FGP porous annular disk without electrical loading on the inner surface and with mechanical pressure on the outer surface.

Figure 6 presents stresses, electric potential, and radial displacement for various values of grading index $n = 4,10,20$ and $n \to \infty$. Fig. 6(a) shows the radial stress on the FGP porous annular disk with different grading indexes. The radial stress equals zero on the internal surface and equals one on the external surface which obeys the mechanical boundary condition. Fig. 6(b) displays the hoop stress on the annular disk with various grading indexes. At the value of $n = 4,10$ the hoop stress decreases along the radial direction while at $n = 20$ and $n \to \infty$ the hoop stress increases from inner to outer surfaces. The electric potential illustrate in Fig. 6(c). The electric potential increasing for all grading index value along the radial domain and decreases near the outer surface to reach zero value. Fig. 6(d) displays the radial displacement. The maximum value of radial displacement happens at $n = 10$. The radial displacement curves decrease from the inner to outer surface at $n = 4,10$ while the radial displacement increases from the internal to external surface at $n = 20$ and $n \to \infty$.

Figure 7 displays the radial stress, hoop stress, electric potential, and radial displacement with various values of porosity parameter β. Fig. 7(a) shows the radial stress with different porosity parameters. All curves of radial stress are semi-coincide. The radial stress is decrescent along the radial direction of the FGP porous annular disk from zero to -1. Fig. 7(b) illustrates the hoop stress along with the radial domain in the annular porous disk. The hoop stress increases and then decreases for $\beta = 0, 0.2, 0.3$ while at $\beta = 0.2$ the hoop stress is decreasing along the radius of the disk. The electric potential is shown in Fig. 7(c) with various porosity parameters. All curves are increasing from zero at the inner surface and then decrease near the outer surface to zero to accept the electric boundary condition. Fig. 7(d) displays the radial displacement on the FGP porous annular disk. The maximum value of radial displacement occurs at $\beta = 0.1$ and the minimum value at $\beta = 0.2$.

4.3 Example 3: Electric-Free Conditions

The FGP porous annular rotating disk applied electric potential on the inner surface and grounded on the other surface. Free of mechanical loading on the annular disk. The rotating disk in this caste treating as an actuator. Suppose the dimensionless in the form:

$$\{\bar{\sigma}_r, \bar{\sigma}_\theta, \bar{\psi}\} = \left\{\sigma_r, \sigma_\theta, \frac{\psi}{\psi_1}\right\}. \tag{33}$$

Table 4 recorded the comparison data between perfect and porous FGP annular disks with distinct values of grading index

n and the exact value of radius for displacement, stresses, and electric potential. Clear from the table data that the values in the perfect FGP annular disk are greater than the porous values for displacement, stresses, and electric potential.

Table 4: Effects of porosity parameter and grading index on FGP porous annular disk with an electrical load on the internal surface and without mechanical pressure on the external surface.

Variable	$\bar{r}$		Perfect FGPM ($\beta = 0$)			Porous FGPM ($\beta = 0.2$)		
			$n = 5$	$n = 10$	$n = 20$	$n = 5$	$n = 10$	$n = 20$
$\bar{u}$	0.3		0.14267	-0.56361	-1.0374	-0.67219	-1.1962	-204.24
	0.5		0.56687	0.10259	-0.20786	0.00654	-0.34583	-139.62
	0.7		0.96342	0.62381	0.40082	0.53852	0.27008	-106.78
$\bar{\sigma}_r$	0.3		0.05441	-0.02158	-0.07240	-0.03486	-0.08425	-19.657
	0.5		0.10680	0.03407	-0.01441	0.00860	-0.04064	-19.920
	0.7		0.10682	0.05828	0.02484	0.03279	-0.00449	-15.165
$\bar{\sigma}_\theta$	0.3		0.24234	0.09389	-0.00513	0.01972	-0.05843	-39.502
	0.5		0.30470	0.26989	0.24709	0.20599	0.17936	-11.831
	0.7		0.31842	0.31953	0.31989	0.25426	0.25022	-3.5286
$\bar{\psi}$	0.3		0.97243	0.90163	0.85370	0.92412	0.88074	-14.930
	0.5		0.96375	0.74968	0.60495	0.79366	0.65594	-50.673
	0.7		0.97909	0.66028	0.43916	0.70420	0.50162	-80.155

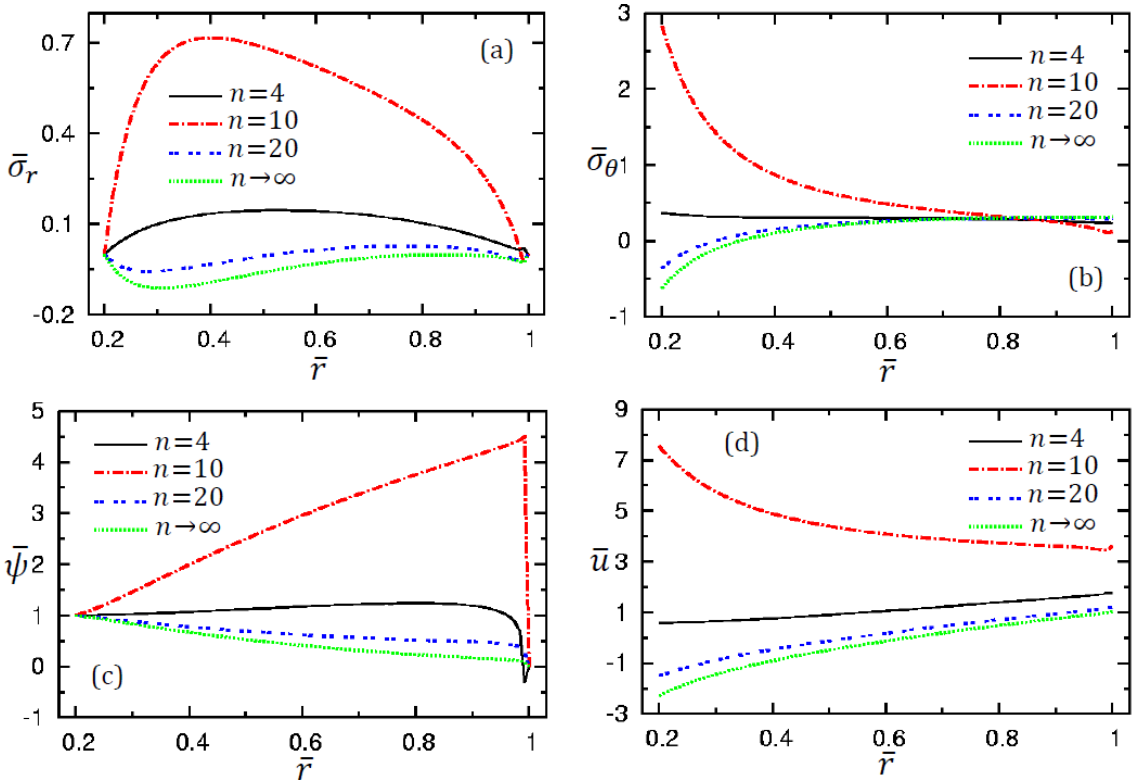

Fig. 8: Grading index effect on stresses, electric potential, and displacement on FGP porous annular disk with free mechanical pressure and electrical load on the inner surface.

Figure 8 illustrates the radial stress, hoop stress, electric potential, and radial displacement with different values of the grading index. Fig. 8(a) displays the radial stress which accepts the boundary conditions equivalent to zero on the internal and external surfaces of the FGP porous annular disk. Fig. 8(b) demonstrates the hoop stress along the radii. The greatest value of the hoop stress occurs at $n = 10$ and the lower value at $n \to \infty$ on the inner surface. On the outer ones, the

greatest value of hoop stress happens at $n \to \infty$ and the minimum value at $n = 10$. The electric potential is presented in Fig. 8(c). The electric potential increases during the radii and suddenly decreases to obey the electric boundary conditions. Fig. 8(d) presents the behavior of radial displacement. The greatest value of radial displacement occurs when $n = 10$ and the minimum value when $n \to \infty$.

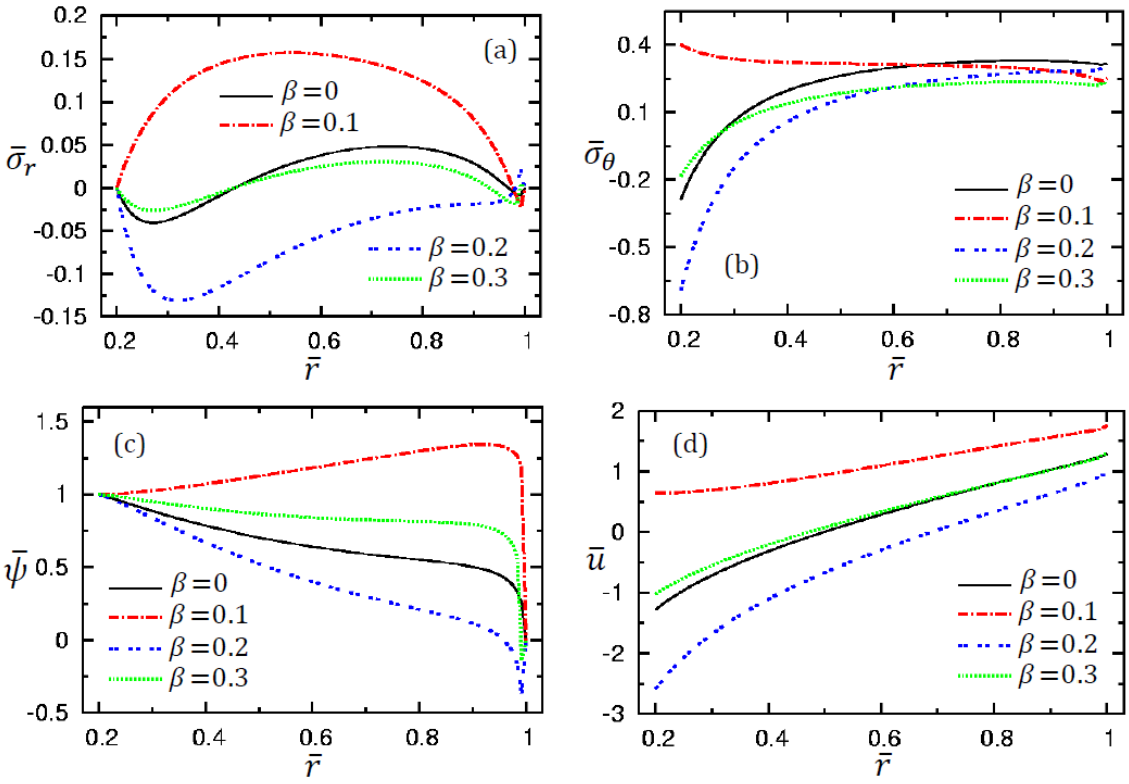

Fig. 9: Porosity parameter effect on stresses, electric potential, and displacement on FGP porous annular disk with free mechanical pressure and electrical load on the inner surface.

Figure 9 shows the radial stress, hoop stress, electric potential, and radial displacement for various values of grading index and porosity parameter $\beta = 0.1$. Fig. 9(a) displays the radial stress along with the radial domain. the radial stress curves equal zero on the internal and external surfaces which satisfies the mechanical boundary conditions. Fig. 9(b) presents the hoop stress on the FGP porous annular disk with various values of porosity parameter. The hoop stress has a maximum value when $\beta = 0.1$ and a minimum value when $\beta = 0.2$ on the inner surface. At the outer surface, the maximum value of hoop stress occurs at $\beta = 0$ and the lower value at $\beta = 0.3$. The electric potential is presented in Fig. 9(c). The electric potential increases during the radii and suddenly decreases to obey the electric boundary conditions. The radial displacement is displayed in Fig. 9(d). The radial displacement increases during the disk radius. The maximum value of radial displacement occurs at $\beta = 0.1$ and the minimum value at $\beta = 0.2$.

4.4 Example 4: Mechanical-Electric Conditions

The last example is the general case of combining mechanical and electrical loading on the FGP porous annular disk with variable thickness. The dimensionless stresses and electric potential can be written in the form

$$\{\bar{\sigma}_r, \bar{\sigma}_\theta, \bar{\psi}\} = \left\{\frac{\sigma_r}{P_1}, \frac{\sigma_\theta}{P_1}, \frac{\psi}{\psi_2}\right\}. \tag{34}$$

Table 5 displays the numerical data of radial displacement, stresses, and electric potential with different values of grading index and two exact values of porosity parameter in the case of the perfect and porous annular disk. From the table data, all numerical values in the case of the perfect annular disk are greater than the corresponding ones of the porous disk.

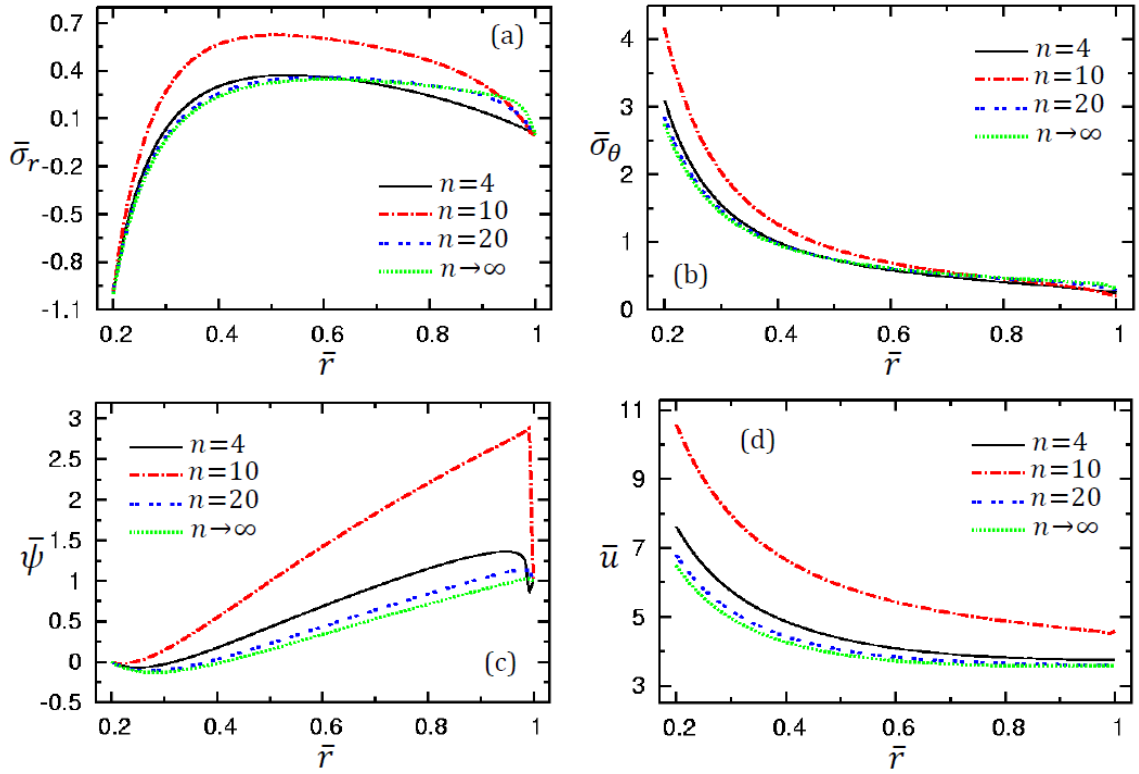

Fig. 10: Grading index effect on stresses, electric potential, and displacement on FGP porous annular disk with mechanical pressure on the internal surface and electrical load on the external surface.

Table 5: Effects of porosity parameter and grading index on FGP porous annular disk with mechanical pressure on the internal surface and electrical load on the external surface.

Variable	$\bar{r}$	Perfect FGPM ($\beta = 0$)			Porous FGPM ($\beta = 0.2$)		
		$n = 5$	$n = 10$	$n = 20$	$n = 5$	$n = 10$	$n = 20$
$\bar{u}$	0.3	5.2121	4.95732	4.7896	5.1988	4.4084	-82.302
	0.5	4.0161	3.87291	3.7785	4.0014	3.1856	-55.957
	0.7	3.6401	3.55701	3.5074	3.4644	3.5122	-42.401
$\bar{\sigma}_r$	0.3	0.02396	0.00108	-0.01409	-0.02966	-0.04355	-8.4973
	0.5	0.37347	0.36016	0.34929	0.31097	0.30619	-8.2740
	0.7	0.33681	0.35337	0.35246	0.28616	0.30863	-6.2295
$\bar{\sigma}_\theta$	0.3	1.5526	1.51361	1.4879	1.4220	1.4009	-15.628
	0.5	0.76095	0.76630	0.76934	0.68533	0.69347	-4.4845
	0.7	0.51679	0.53908	0.55158	0.46077	0.48102	-1.1404
$\bar{\psi}$	0.3	-0.03228	-0.06724	-0.09015	-0.10117	-0.12713	-6.963
	0.5	0.37652	0.27899	0.21406	0.25580	0.18370	-22.001
	0.7	0.83592	0.69786	0.60184	0.69342	0.59624	-34.265

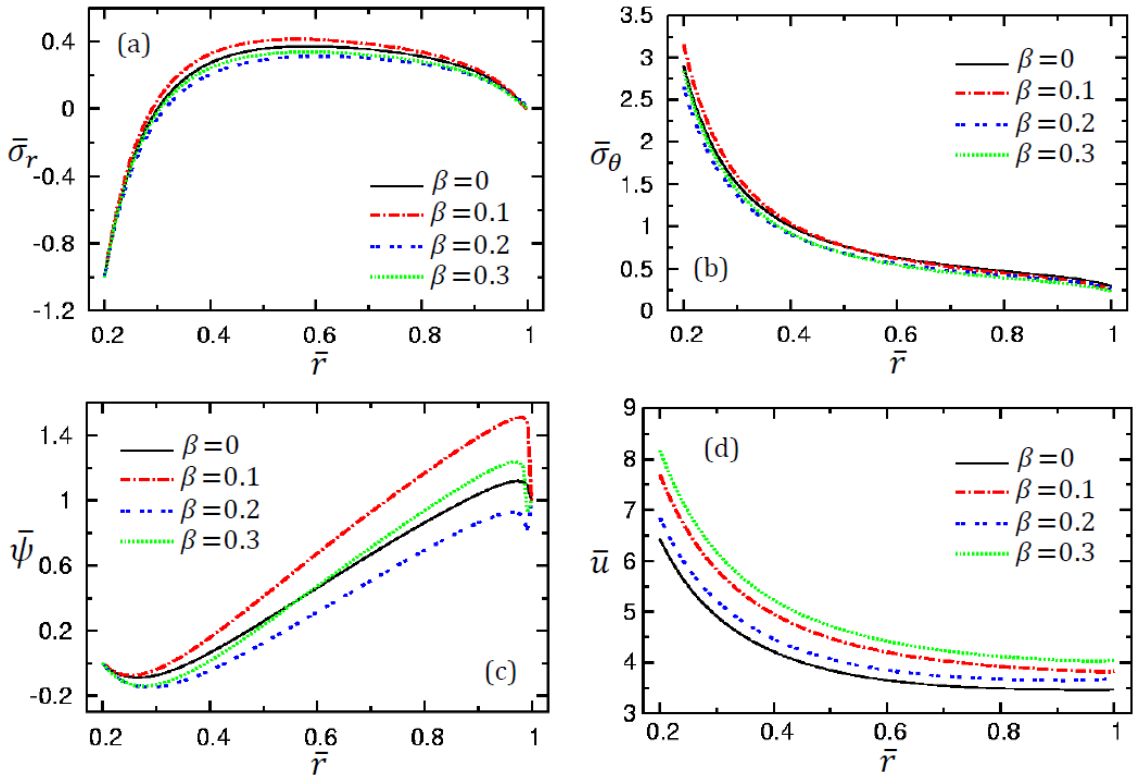

Fig. 11: Porosity parameter effect on stresses, electric potential, and displacement on FGP porous annular disk with mechanical pressure on the internal surface and electrical load on the external surface.

Figure 10 shows the stresses, electric potential, and displacement with various grading index values. Fig. 10(a) displays the radial stress along the radius of the disk with the various grading index values and the value of porosity factor $\beta = 0.1$. The radial stress satisfies the boundary conditions equal to -1 on the internal surface and equal to zero on the external one. Fig. 10(b) demonstrates the hoop stress along the radial direction. All curves of hoop stress decrease from the inner surface to the external radius. The electric potentials are displayed in Fig. 10(c) with different values of n. Also, the electric potential satisfies the boundary conditions, equal one on the outer surface and vanish on the inner surface. Fig. 10(d) displays the radial displacement with various grading index values. The radial displacement is decreasing along the radial direction of the FGP porous annular disk.

Figure 11 displays the radial stress, hoop stress, electric potential, and radial displacement with various values of porosity parameter β and the grading index value $n = 12$. Fig. 11(a) shows the radial stress with different porosity factors. All radial stress is semi-coinciding and obeys the mechanical boundary condition equal to one on the internal radius and vanishes on the external surface. Fig. 11(b) illustrates the hoop stress, notice that the hoop stress is decreased along the radial direction. Fig. 11(c) shows the effect of electric potential with various values of β. The electric potential increases and then decreases near the external surface to accept the electric boundary conditions. The radial displacement is illustrated in Fig. 11(d). The radial displacement decreases along the radial direction. The maximum value of radial displacement occurs when $\beta = 0.3$ and the minimum value when $\beta = 0$. It is important to mention here to the fact that the above results can be used in different applications [38-46].

5 Conclusions

This article studies magneto-electric-hygrothermal effects on rotating variable-thickness porous FG annular disks under various loading of mechanical pressure, electric potential, and hygrothermal distribution. A semi-analytical solution is used to solve the equilibrium differential equations and Maxwell equations. From the numerical results, we can deduce that:

- The grading index n and the porosity parameter β have a great influence on the stress's values, electric potential, and displacement.
- The semi-analytical method is very effective and important to solve the same problem in solving differential equations.

- From the table data, the values of stresses, electric potential, and displacement in the case of a perfect FGP annular disk are greater than the corresponding values in the porous FGP annular disk with different sets of boundary conditions.
- Choosing the suitable values of grading index and porosity factor on the rotating annular disk with variable thickness helps the designers to control the stresses and displacement values.
- The complex mathematical model is very useful to design an annular rotating disk with loading combinations.

Acknowledgment

All thanks and appreciation to the spirit of Prof. Dr. Mohamed Nabil Allam for his continuous support of the authors.

Conflict of interest

The authors declare that there is no conflict regarding the publication of this paper.

References

[1] A. Gupta, M. Talha, Influence of initial geometric imperfections and porosity on the stability of functionally graded material plates, Mech. Based Des. Struct., 46(6), 693-711 (2018). Doi: 10.1080/15397734.2018.1449656

[2] Y.Q. Wang, J.W. Zu, Vibration characteristics of moving sigmoid functionally graded plates containing porosities, Int. J. Mech. Mater., 14, 473–489 (2018). Doi: 10.1007/s10999-017-9385-2

[3] Y.Q. Wang, Y.E. Chao, J.W. Zu, Identifying the temperature effect on the vibrations of functionally graded cylindrical shells with porosities, Appl. Math. Mech., **39(11)**, 1587–1604 (2018). Doi: 10.1007/s10483-018-2388-6

[4] S.F. Nikrad, A. Kanellopoulos, M. Bodaghi, Z.T. Chen, Large deformation behavior of functionally graded porous curved beams in thermal environment, Arch. Appl. Mech., **91**, 2255–2278 (2021). Doi: 10.1007/s00419-021-01882-9

[5] M. Jabbari, S. Karampour, M.R. Eslami, Steady state thermal and mechanical stresses of a poro-piezo-FGM hollow sphere, Meccanica, **48**, 699-719 (2013). Doi: 10.1007/s11012-012-9625-3

[6] D.S. Mashat, A.M. Zenkour, A.F. Radwan, A quasi-3D higher-order plate theory for bending of FG plates resting on elastic foundations under hygro-thermo-mechanical loads with porosity, Eur J Mech A Solids, **82**, 103985 (2020). Doi: 10.1016/j.euromechsol.2020.103985

[7] I. Mechab, B. Mechab, S. Benaissa, B. Serier, B. Bouiadjra Bachir, Free vibration analysis of FGM nanoplate with porosities resting on Winkler Pasternak elastic foundations based on two-variable refined plate theories, J. Braz. Soc. Mech. Sci. Eng., **38**, 2193–2211 (2016). Doi: 10.1007/s40430-015-0482-6

[8] F. Ebrahimi, M. Mokhtari, Transverse vibration analysis of rotating porous beam with functionally graded microstructure using the differential transform method, J. Braz. Soc. Mech. Sci. Eng., **37(4)**, 1435–1444 (2015). Doi:10.1007/s40430-014-0255-7

[9] F. Ebrahimi, E. Salari, Thermo-mechanical vibration analysis of nonlocal temperature-dependent FG nanobeams with various boundary conditions, Compos. B. Eng., **78**, 272–290 (2015). Doi: 10.1016/j.compositesb.2015.03.068

[10] D. Chen, J. Yang, S. Kitipornchai, Free and forced vibrations of shear deformable functionally graded porous beams, Int. J. Mech. Sci., **108–109**, 14–22 (2016). Doi: 10.1016/j.ijmecsci.2016.01.025

[11] Y. Wang, D. Wu, Free vibration of functionally graded porous cylindrical shell using a sinusoidal shear deformation theory, Aerosp Sci Technol, **66**, 83–91 (2017). Doi: 10.1016/j.ast.2017.03.003

[12] D. Wu, A. Liu, Y. Huang, Y. Huang, Y. Pi, W. Gao, Dynamic analysis of functionally graded porous structures through finite element analysis, Eng. Struct., **165**, 287–301 (2018). Doi: 10.1016/j.engstruct.2018.03.023

[13] M. Jabbari, M. Hashemitaheri, A. Mojahedin, M.R. Eslami, Thermal buckling analysis of functionally graded thin circular plate made of saturated porous materials, J. Therm. StresseS, **37**, 202–220 (2014). Doi: 10.1080/01495739.2013.839768

[14] A.M. Zenkour, M.H. Aljadani, Porosity effect on thermal buckling behavior of actuated functionally graded piezoelectric nanoplates, Eur J Mech A Solids, **78**, 103835 (2019). Doi: 10.1016/j.euromechsol.2019.103835

[15] A.A. Daikh, A.M. Zenkour, Effect of porosity on the bending analysis of various functionally graded sandwich plates, Mater. Res. Express., **6**, 065703 (2019). Doi:10.1088/2053-1591/ab0971

[16] R. Tantawy, A.M. Zenkour, Effect of Porosity and Hygrothermal Environment on FGP Hollow Spheres under Electromechanical Loads, J. Appl. Comput. Mech., **8(2)**, 710–722 (2022). Doi: 10.22055/JACM.2021.39229.3377

[17] M.N.M. Allam., R.E. Badr, R. Tantawy, Stresses of a rotating circular disk of variable thickness carrying a current and bearing a coaxial viscoelastic coating, Appl. Math. Model., **32**, 1643-1656 (2008). Doi: 10.1016/j.apm.2007.06.002

[18] T. Dai, H.L. Dai, Z.Y. Lin, Multi-field mechanical behavior of a rotating porous FGMEE circular disk with variable thickness under hygrothermal environment, Compos. Struct., **210**, 641–656 (2019). Doi: 10.1016/j.compstruct.2018.11.077

[19] A.M. Zenkour, Stress distribution in rotating composite structures of functionally graded solid disks, J. Mater. Process. Technol., **209**, 3511-3517 (2009). Doi: 10.1016/j.jmatprotec.2008.08.008

[20] M.N.M. Allam, R. Tantawy, A.M. Zenkour, Thermoelastic stresses in functionally graded rotating annular disks with variable thickness, J. Theor. Appl. Mech., **56(4)**, 1029–1041 (2018). Doi: 10.15632/jtam-pl.56.4.1029

[21] M. Bayat, M. Rahimi, M. Saleem, A.H. Mohazzab, I. Wudtke, H. Talebi, One dimensional analysis for magneto-thermo-mechanical response in a functionally graded annular variable-thickness rotating disk, Appl. Math. Model., **38(19)**, 4625-4639 (2014). Doi: 10.1016/j.apm.2014.03.008

[22] D. Das, P. Sahoo, K. Saha, Dynamic analysis of rotating annular disk of variable thickness under uniform axial pressure, Int. J. Comput. Meth. Eng. Sci. Mech., **13(1)**, 37-59 (2012). Doi: 10.1080/15502287.2011.636788

[23] A. Hassani, M.H. Hojjati, E. Mahdavi, R.A. Alashti, G. Farrahi, Thermo-mechanical analysis of rotating disks with non-uniform thickness and material properties, Int. J. Press. Vessel. Pip., **98**, 95-101 (2012). Doi: 10.1016/j.ijpvp.2012.07.010

[24] M.E. Golmakani, Large deflection thermoelastic analysis of shear deformable functionally graded variable thickness rotating disk, Compos. B. Eng., **45**, 1143-1155 (2013). Doi: 10.1016/j.compositesb.2012.08.012

[25] T. Dai, H.L Dai, Investigation of mechanical behavior for a rotating FGM circular disk with a variable angular speed, J. Mech. Sci., **29(9)**, 3779-3787 (2015). Doi: 10.1007/s12206-015-0824-4

[26] Dai T., H.L. Dai, Analysis of a rotating FGMEE circular disk with variable thickness under thermal environment, Appl. Math. Model., **45**, 900-924 (2017). Doi: 10.1016/j.apm.2017.01.007

[27] M. Bayat, B.B. Sahari, M. Saleem, A. Ali, S.V. Wong, Bending analysis of a functionally graded rotating disk based on the first order shear deformation theory, Appl. Math. Model., **33**, 4215-4230 (2009). Doi: 10.1016/j.apm.2009.03.001

[28] M. Bayat, B.B. Sahari, M. Saleem, A. Ali, S.V. Wong, Thermoelastic solution of a functionally graded variable thickness rotating disk with bending based on the first-order shear deformation theory, Thin-Walled Struct., **47**, 568-582 (2009). Doi: 10.1016/j.tws.2008.10.002

[29] M. Bayat, B.B. Sahari, M. Saleem, A.M.S. Hamouda, J.N. Reddy, Thermoelastic analysis of functionally graded rotating disks with temperature-dependent material properties: uniform and variable thickness, Int. J. Mech. Mater. Des., **5** ,263-279 (2009). Doi: 10.1007/s10999-009-9100-z

[30] G. Paria, Magneto-elasticity and magneto-thermo-elasticity, Adv. Appl. Mech., **10(1)**, 73-112 (1967). Doi: 10.1016/S0065-2156(08)70394-6

[31] Y. Ootao, Y Tanigawa, Transient piezothermoelastic analysis for a functionally graded thermopiezoelectric hollow sphere, Compos. Struct., **81**, 540–549 (2007). Doi: 10.1016/j.compstruct.2006.10.002

[32] A. Ghorbanpour Arani, R. Kolahchi, A.A. Mosallaie Barzoki, A. Loghman, Electro-thermo-mechanical behaviors of FGPM spheres using analytical method and ANSYS software, Appl. Math. Model., **36**, 139–157 (2012). Doi: 10.1016/j.apm.2011.05.031

[33] H.L. Dai, H.J. Jiang, Analytical study for electromagnetothermoelastic behavior of a functionally graded piezoelectric solid cylinder, Mech. Adv. Mater. Struct., **20(10)**, 800-811 (2013). Doi: 10.1080/15376494.2012.676715

[34] H.L. Dai, T. Dai, L. Yang, Free vibration of a FGPM circular plate placed in a uniform magnetic field, Meccanica,

48(10), 2339-2347 (2013). Doi: 10.1007/s11012-013-9752-5

[35] M.A. Ezzat, Generation of generalized thermomagnetoelastic waves by thermal shock in a perfectly conducting half-space, J. Therm. Stresses, **20**, 633-917 (1997). Doi: 10.1080/01495739708956121

[36] J.D. Kraus, Electromagnetic, U.S.A: McGraw Hill, Inc. (1984).

[37] H.L. Dai, X. Wang, Dynamic responses of piezoelectric hollow cylinders in an axial magnetic field, Int J Solids Struct, **41**, 5231-5246 (2004). Doi: 10.1016/j.ijsolstr.2004.04.019